Non-linear circuit based model of PMSM under inter-turn fault: a simple approach based on healthy machine data

L. Belguerras[1], J. Arellano-Padilla[1], P. Arumugam[1], T. Hamiti[1], S. Mezani[1] and C. Gerada[1]

[1] University of Nottingham, Faculty of Engineering, PEMC group, Nottingham, NG7 2RD, UK

Abstract The paper proposes a fast dynamic mathematical model to evaluate the performances of saturated permanent magnet synchronous machines (PMSM) under stator winding's inter turn fault. The parameters of the model can be determined using only manufacturer's data of the healthy machine. Two surface mounted PMSM have been considered to investigate the validity of the proposed approach; with distributed and concentrated winding. It has been shown that the proposed model predicts the fault current with a reasonable accuracy compared to the non-linear Finite Elements analyses and to the experimental results. This model can be incorporated in a global simulation environment of power electronic of electrical device since the computation time is very short.

***Index Terms*— Inter-turn fault, finite elements methods, dynamic models, magnetic saturation.**

I. INTRODUCTION

Inter turn fault in the stator winding is the consequence of insulation failures between two turns in the same phase and it is one of the most common fault in electrical machines. This fault results in a very large short circuit current which could lead to the machine breakdown if this current is not quickly detected and eliminated [1, 2]. Furthermore, from a pure modelling aspect, a high short-circuit current causes magnetic saturation of stator yoke. In the literature, many authors have proposed linear circuit models coupled with equivalent magnetic circuits in which the faulty machine is represented by a set of constant inductances and resistances [3, 4]. Unfortunately, these models fail to give satisfactory results in the saturated case. In this case, finite element (FE) analyses of the faulty machine lead to the most precise results. However, FE analyses are very costly in terms of computation time. Furthermore, the machine geometry and the ferromagnetic materials have to be specified.

To reduce the computation time, circuit models extended to the non-linear case, are the preferred methods of analysis of saturated faulty machines. The basic idea is to use a set of inductances which vary with the instantaneous current value as to deal with the saturated case. Obviously, these current-dependent inductances, known as "saturated, incremental or dynamic inductances" need to be determined [5]. When the machine geometry is available, FE methods or permeance networks [6, 7, 8] allow the computation of these inductances under faulty conditions. Another approach consists of representing the faulty machine by a set of non-linear differential equations where a map of the machine's fluxes and their derivatives vs. the different currents are introduced ; their computation being performed by FE, permeance network or winding function theory [9, 10, 11]. However, the use of these approaches requires, again, the knowledge of the machine geometry and the B-H curves of the ferromagnetic materials but the computation time is lower than the full FE analyses. All these works on saturated PM machines under inter-turn faults conditions allow a good prediction of the machine performances as well as the current in the faulty turns. Researchers in this area and experienced engineers are familiar with these approaches which require detailed data of the machine. These details are of course not available for the machine end-user who needs much simple mathematical models with only few data generally given by the manufacturer for the healthy machine.

In the healthy case, many authors [12, 13, 14, 15] have proposed models taking into account the saturation effect by using the d-axis and q-axis machine magnetizing curves which can be given by the manufacturer [16]. By using theses curves, we propose in this paper a fast dynamic mathematical model of PMSM under inter turn fault. The presented model is the extension, to the saturated case, of the simple linear model of PMSM under inter-turn fault condition. This model whose parameters are obtained from manufacturer's data allows an evaluation of the saturated PMSM performances under inter-turn fault.

II. CLASSICAL LINEAR MODEL OF PMSM UNDER INTER-TURN FAULT

In linear conditions, the classical dynamic model of PMSM under inter turn short circuit can be developed in abc or dq frame. Assuming that a short circuit occurs in phase "a" Fig. 1, the modelling of the shorted turns fault requires the introduction of an additional differential equation associated to the shorted turn [17, 18, 19, 20]. Thus, phase 'a' will be divided into two windings whose resistances R_{a1} and R_{a2} are proportional to the number of short-circuited turns. They are expressed in term of the healthy machine phase resistance R and the ratio $\mu=N_{tsh}/N_t$ between the number of shorted turns and the number of total phase turns by $R_{a2} = \mu R$ and $R_{a1} = (1-\mu) R$.

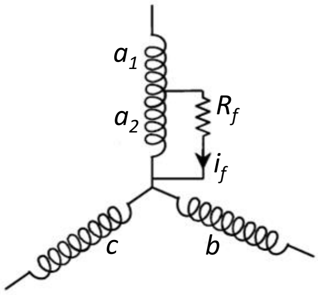

Fig. 1. Three phase winding under inter-turn fault in phase 'a'

The additional circuit is modelled as an additional phase winding magnetically coupled to all the other phases of the machine. Indeed, the self and the mutual inductances of the additional faulty circuit are related to the healthy machine inductance L and the ratio μ.

The self-inductance of the faulty part of phase 'a', the mutual inductances between the faulty part and the phases 'a' and 'b' and the mutual inductance between the faulty part (coil a_2) and the healthy one (coil a_1) are expressed by [17]

$$L_{a2} = \mu^2 L \ ; \ M_{a2b} = M_{a2c} = \mu M \ ; \ M_{a1a2} = \mu(1-\mu) L \tag{1}$$

Where L and M are the phase self and mutual inductances of the healthy machine respectively.

In reality, the relations given in (1) assume that the machine has only one coil per phase. In the case of multipolar and/or distributed winding, the use of (1) is not strictly valid because the « faulty turns coil » is not necessary aligned with the axis of the faulty phase. Nevertheless, owing to their simplicity, many authors used relations (1) for modelling interturn faults in electrical machines (including fractional slot windings) [7], [19] and [20]. The obtained results were not far from those computed using finite element analyses.

In this study, we adopt the same relations (1) to compute the parameters of faulty surface mounted permanent magnet machine and we will show how the linear model is extended to the saturated case.

To establish the machine's equations, iron losses, damping effects and all eddy currents are neglected. For an unsaturated surface mounted PMSM, the electrical model in (*abc*) frame describing the circuit in Fig.1, can be written as

$$\begin{bmatrix} V_{a1} \\ V_{a2} \\ V_b \\ V_c \end{bmatrix} = \begin{bmatrix} R_{a1} & 0 & 0 & 0 \\ 0 & R_{a2} & 0 & 0 \\ 0 & 0 & R_b & 0 \\ 0 & 0 & 0 & \mathrm{R_c} \end{bmatrix} \begin{bmatrix} i_a \\ i_a - i_f \\ i_b \\ i_c \end{bmatrix} + \begin{bmatrix} L_{a1} & \mathrm{M_{a1a2}} & \mathrm{M_{a1b}} & \mathrm{M_{a1c}} \\ \mathrm{M_{a1a2}} & \mathrm{L_{a2}} & \mathrm{M_{a2b}} & \mathrm{M_{a2c}} \\ \mathrm{M_{a1b}} & \mathrm{M_{a2c}} & \mathrm{L_b} & \mathrm{M_{bc}} \\ \mathrm{M_{a1c}} & \mathrm{M_{a2c}} & \mathrm{M_{bc}} & \mathrm{L_c} \end{bmatrix} \frac{d}{dt} \begin{bmatrix} i_a \\ i_a - i_f \\ i_b \\ i_c \end{bmatrix} + \begin{bmatrix} e_{a1} \\ e_{a2} \\ e_b \\ e_c \end{bmatrix} \tag{2}$$

According to (2) and to the circuit of Fig.1, the voltage of phase 'a' is

$$V_a = V_{a1} + V_{a2} \tag{3}$$

With

V_{a1} is the voltage in the healthy part (coil 'a_1')

V_{a2} is the voltage in the faulty part (coil 'a_2'), it is given by

$$V_{a2} = R_f \, i_f \tag{4}$$

i_f is the fault current through the insulation fault resistance R_f which depends on the failure severity. R_f is very high in the healthy case (several Mega Ohms).

The fault current i_f is a new state variable. Indeed, the modelling requires the introduction of an additional differential equation associated to the shorted turn. From the circuit presented in Fig.1, the equation of the fault loop is given by

$$0 = R_{a2}.i_a + (L_{a2} + M_{a1a2})\frac{di_a}{dt} + M_{a2b}\frac{di_b}{dt} + M_{a2c}\frac{di_c}{dt} - (R_{a2} + R_f)i_f - L_{a2}.\frac{di_f}{dt} + e_{a2} \quad (5)$$

For the balanced healthy PMSM, we have

$$R_{a1} + R_{a2} = R_b = R_c = R \quad (6)$$

$$L_{a1} + L_{a2} + 2M_{a1a2} = L_b = L_c = L \quad (7)$$

$$M_{a1b} + M_{a2b} = M_{a1c} + M_{a2c} = M_{bc} = M \quad (8)$$

$$e_a = e_{a1} + e_{a2} = e_b = e_c \quad (9)$$

By considering these last equations, (2) can be rewritten as

$$V_{abcf} = R_{abcf}\, i_{abcf} + L_{abcf}\frac{di_{abcf}}{dt} + e_{abcf} \quad (10)$$

Where the inductance matrix is

$$L_{abcf} = \begin{bmatrix} L_s & 0 & 0 & -(L_{a2} + M_{a1a2}) \\ 0 & L_s & 0 & -M_{a2b} \\ 0 & 0 & L_s & -M_{a2c} \\ -(L_{a2} + M_{a1a2}) & -M_{a2b} & -M_{a2c} & L_{a2} \end{bmatrix} \quad (11)$$

$L_s = L - M$ is the cyclical inductance.

V_{abcf}, i_{abcf} and e_{abcf} are the stator voltage, current and back-EMF vectors, respectively. They are expressed by

$$V_{abcf} = [V_a\ V_b\ V_c\ 0]^T\ ;\ i_{abcf} = [i_a\ i_b\ i_c\ i_f]^T\ ;\ e_{abcf} = [e_a\ e_b\ e_c\ e_f]^T \quad (12)$$

The resistance matrix R_{abcf} is

$$R_{abcf} = \begin{bmatrix} R & 0 & 0 & -R_{a2} \\ 0 & R & 0 & 0 \\ 0 & 0 & R & 0 \\ -R_{a2} & 0 & 0 & R_{a2} + R_f \end{bmatrix} \quad (13)$$

e_f is the back-EMF of the faulty turns (coil a2). It is expressed in term of the ratio μ by

$$e_f = -\mu\, e_a \quad (14)$$

The back-EMFs in the three phases e_{abcf} can be expressed as

$$e_{abcf} = p\Omega \frac{d\Phi_{abcf}}{d\theta_e} \tag{15}$$

$\theta_e = p\theta$ is the electrical angle, Ω is the mechanical angular speed ($\Omega = d\theta / dt$) and p the number of pole pairs.

Φ_{abcf} is the flux linkage vector due to the permanent magnets expressed by

$$\Phi_{abcf} = [\Phi_a, \Phi_b, \Phi_c, \Phi_f] = \Phi_m[\sin(\theta_e), \sin(\theta_e - 2\pi/3), \sin(\theta_e + 2\pi/3), -\mu\sin(\theta_e)] \tag{16}$$

With Φ_f is the flux through to the faulty part (coil 'a$_2$') and Φ_m is the magnet flux linkage

Equations (10) – (12) clearly show that the faulty machine model can be separated into a healthy part and a faulty one. The two part being electrically coupled. Hence, one can use an extended Park transform to the machine in which the Concordia T_{43} and the rotation $P(\theta_e)$ matrices contain an additional elements to account for the faulty part. These transformation matrices are

$$T_{43}^t = \sqrt{\frac{2}{3}} \begin{bmatrix} 1 & -\frac{1}{2} & -\frac{1}{2} & 0 \\ 0 & \frac{\sqrt{3}}{2} & -\frac{\sqrt{3}}{2} & 0 \\ 0 & 0 & 0 & \sqrt{\frac{3}{2}} \end{bmatrix} \; ; \; P(\theta_e) = \begin{bmatrix} \cos(\theta_e) & -\sin(\theta_e) & 0 \\ \sin(\theta_e) & \cos(\theta_e) & 0 \\ 0 & 0 & 1 \end{bmatrix} \tag{17}$$

Then, applying the transformation to (10), one obtains in the dq reference frame

$$V_{dqf} = R_{dqf}\, i_{dqf} + L_{dqf} \frac{di_{dqf}}{dt} + L_{dqf}\, P(-\theta_e) \frac{d}{d\theta_e} P(\theta_e) i_{dqf} + e_{dqf} \tag{18}$$

With

$$\begin{gathered} V_{dqf} = P(-\theta_e)\, T_{43}^t V_{abcf} \;\; ; i_{dqf} = P(-\theta_e)\, T_{43}^t i_{abcf} \;\; ; \; e_{dqf} = P(-\theta_e)\, T_{43}^t e_{abcf} \\ R_{dqf} = P(-\theta_e)\, T_{43}^t R_{abcf}\, T_{43} P(\theta_e) ; \; L_{dqf} = P(-\theta_e)\, T_{43}^t L_{abcf}\, T_{43} P(\theta_e) \end{gathered} \tag{19}$$

The voltage equations in dq frame are then

$$\begin{cases} V_d = R\, i_d - L_q p\Omega i_q + L_d \frac{di_d}{dt} - \mathrm{R}'_{a2} \cos(\theta_e) i_f + (M_{fa}\cos(\theta_e) + M_{fb} sin(\theta_e)) \frac{di_f}{dt} + e_d \\ V_q = R\, i_q - L_d p\Omega i_d + L_q \frac{di_q}{dt} + \mathrm{R}'_{a2} \sin(\theta_e) i_f + (M_{fb}\cos(\theta_e) - M_{fa} sin(\theta_e)) \frac{di_f}{dt} + e_q \\ 0 = -\mathrm{R}'_{a2} \cos(\theta_e) i_d + (M_{fb}\cos(\theta_e) - M_{fa} sin(\theta_e)) p\Omega i_d + (M_{fa}\cos(\theta_e) + M_{fb}\sin(\theta_e)) \frac{di_d}{dt} + \\ \quad R'_{a2}\, \sin(\theta_e) i_q + (M_{fb} sin(\theta_e) - M_{fa}\cos(\theta_e)) p\Omega i_q + (M_{fb}\cos(\theta_e) - M_{fa} sin(\theta_e)) \frac{di_q}{dt} + \\ \quad R_{fa2} i_f + L_{a2} \frac{di_f}{dt} + e_f \end{cases} \tag{20}$$

In (20), $L_d = L_q = L_s$ as unsaturated, smooth air-gap PMSM is considered. The other parameters are given by

$$R'_{a2} = \sqrt{2/3}\; R_{a2} \;\; ; \;\; R_{fa2} = R_{a2} + R_f \tag{21}$$

$$M_{fa} = 1/\sqrt{6}\, \left(-2(L_{a2} + M_{a1a2}) + M_{a2b} + M_{a2c}\right) \; ; \; M_{fb} = 1/\sqrt{2}\, \left(-M_{a2b} + M_{a2c}\right) \tag{22}$$

The stator winding of the PMSM under inter-turn fault is composed of two balanced parts in dq frame supplied by the phase currents (i_d and i_q) and a faulty winding supplied by the fault current i_f. The electromagnetic torque is expressed as

$$\Gamma_e = \frac{e_d\, i_d + e_q i_q - e_f i_f}{\Omega} \tag{23}$$

III. Saturated Dynamic Mathematical Model Under Inter-turn Fault

In the voltage equations (20) under linear conditions, the inductances along the d and the q axes are constant ($L_d = L_q = L_s$). This is not anymore the case under saturated conditions. One approach commonly used to consider the saturation effect is to introduce dynamic inductances noted ($\hat{L}_d, \hat{L}_q$) instead of (L_d, L_q) respectively. These inductances are obtained from the time derivatives of the dq components of the flux linkage as follows

$$\frac{d}{dt}\psi_d(i_d) = \frac{d\psi_d(i_d)}{di_d}.\frac{di_d}{dt} = \hat{L}_d(i_d)\frac{di_d}{dt} \tag{24}$$

$$\frac{d}{dt}\psi_q(i_q) = \frac{d\psi_q(i_q)}{di_q}.\frac{di_q}{dt} = \hat{L}_q(i_q)\frac{di_q}{dt} \tag{25}$$

Regarding the faulty turns circuit, its self and mutual inductances are related, as shown by (1), to the self-inductance L of the healthy machine. The simple approach introduced here is to use, in (1), an equivalent differential inductance $\hat{L}$ instead of the healthy phase inductance L.

The mutual inductance in PMSM with a concentrated winding can be neglected, so the phase inductance is the same as the d-axis inductance which can be determined from the d-axis flux.

For distributed winding PMSM, the phase inductance can be calculated by assuming a constant flux leakage coefficient between two stator phases. Hence, we introduce the following constant coefficient

$$k = -\frac{M}{L} \tag{26}$$

The phase inductance of the healthy machine is then

$$\hat{L}(i_a) = \frac{1}{1+k} L_d(i_a) \tag{27}$$

Notice that the current i_a is obtained by inverse Park transformation from i_d and i_q.

To summarize, one can say that the saturation effect is considered by simply substituting the linear inductances given above in (1) by the dynamic ones calculated from the $\Psi_d(i_d)$ and $\Psi_q(i_q)$ curves of the healthy machine. These curves can be given by the manufacturer according to the IEEE standard [16], so an end-user does not need to use any numerical calculations. Alternatively, these curves can be obtained from a simple experimental procedure. This will be described later. It is also important to note that this non-linear model does not consider the cross saturation effect.

To implement the method in simulation, one can use a look-up table to compute the measured $\Psi_d(i_d)$ and $\Psi_q(i_q)$ curves. In our case, we used the following approximation of the flux-current curves

$$\Psi(i) = a_1 \arctan(a_2\, i) + a_3\, i \tag{28}$$

From (28), we can derive the dynamic inductance expression as

$$\hat{L}(i) = \frac{d\Psi(i)}{di} = \frac{a_1 a_2}{1 + a_2^2 i^2} + a_3 \tag{29}$$

Where

i represents either i_d or i_q

a_1, a_2 and a_3 are unknown coefficients identified, as shown later, using least squares.

IV. Model Validation

To investigate the validity of the proposed approach, two surface mounted permanent magnet synchronous machines (PMSM) are considered; with distributed winding and with concentrated (fractional-slot) winding.

For the PMSM with distributed winding, the geometry is known. In this case, the d-axis and q-axis magnetization curves are computed for different d-axis and q-axis currents.

For the PMSM with concentrated winding, the geometry is unknown. In order to overcome this problem, the $\Psi_d(i_d)$ and $\Psi_q(i_q)$ curves are obtained by using a simple experiment which will be described later.

The main parameters of this machine in healthy condition and at rated operation are presented in Table I.

Table I Parameters of the studied machines

Parameter	PMSM with concentrated winding	PMSM with distributed winding
Pole pairs, p	14	4
Number of slots, N_s	24	24
Phase inductance (linear case), L (mH)	2.3	3.1
Mutual inductance, M (mH)	-0.05	-0.35
Phase resistance, R (Ω)	0.8	0.44
Series turns per phase, N_t	64	40
Magnets flux linkage, Ψ_m (Wb)	0.0821	0.081
Moment of inertia, J (kg.m^2)	0.0019	0.018
Rated speed, N (rpm)	5000	1000
Rated torque, Γ (Nm)	15	11

A. Finite elements validation (PMSM with distributed winding)

The parameter k given by (26) is then k=0.125. A FE simulation under the usual 2D plane assumption is performed to validate the proposed model. The main geometrical specifications of the machine are given in Fig. 2. The used permanents magnets are NdFeB with a remanence flux density B_r=1.2 T.

To consider the saturation effect, we use the non-linear d-q axes fluxes vs. the corresponding d-q currents, $\Psi_d(i_d)$ and $\Psi_q(i_q)$. As indicated above, we can use a simple experimental procedure to obtain these curves. It will be described later. Here, a 2-D non-linear FE analysis is used to obtain these curves.

Fig. 3 shows the curves $\Psi_d(i_d)$ and $\Psi_q(i_q)$ computed using non-linear FE analysis for different currents i_d and i_q. The variation of the d-axis flux is calculated by subtracting the flux Ψ_m of the PMs ($\Psi_m = \Psi_d(i_d=0,\ i_q=0)$) from the total d-axis flux $\Psi_d(i_d,\ i_q$=constant).

It can be seen that the magnetizing curves $\Psi_d(i_d)$ and $\Psi_q(i_q)$ have the same tendency and they are almost the same for different currents i_d and i_q . Also, the d-axis magnetizing curves are note symmetrical due to the presence of the PMs flux.

The curve $\Psi_d(i_d)$ is computed for $i_q=0$ and the curve $\Psi_q(i_q)$ for i_d=0, then they are approximated by the fitness function (28). As it is shown in Fig. 3-b, the curve $\Psi_q(i_q)$ is symmetrical, so it is approximated by (30) and (31).

The dynamic inductances $L_d\ (i_d)$ and $L_q(i_q)$ calculated by (29) from $\Psi_d(i_d,\ i_q=0)$ and $\Psi_q(i_q,\ i_d=0)$ are presented in Fig. 3-c and Fig. 3-d respectively.

$$\Psi_q(i_q) = 0{,}16 \arctan\left(2{,}13\,.10^{-2}\, i_q\right) + 1{,}145\ 10^{-4} i_q \tag{30}$$

$\Psi_d(i_d)$ curve being not symmetrical, the used fitness function is

$$\Psi_d(i_d) = \begin{cases} 6.87\ 10^{-2} \arctan\left(4{,}57\,.10^{-2}\, i_d\right) + 2{,}04\ 10^{-4} i_d & \text{if } i_d > 0 \\ 0{,}698 \arctan\left(7{,}689\,.10^{-3}\, i_d\right) - 1.85\ 10^{-4}\ i_d & \text{if } i_d < 0 \end{cases} \tag{31}$$

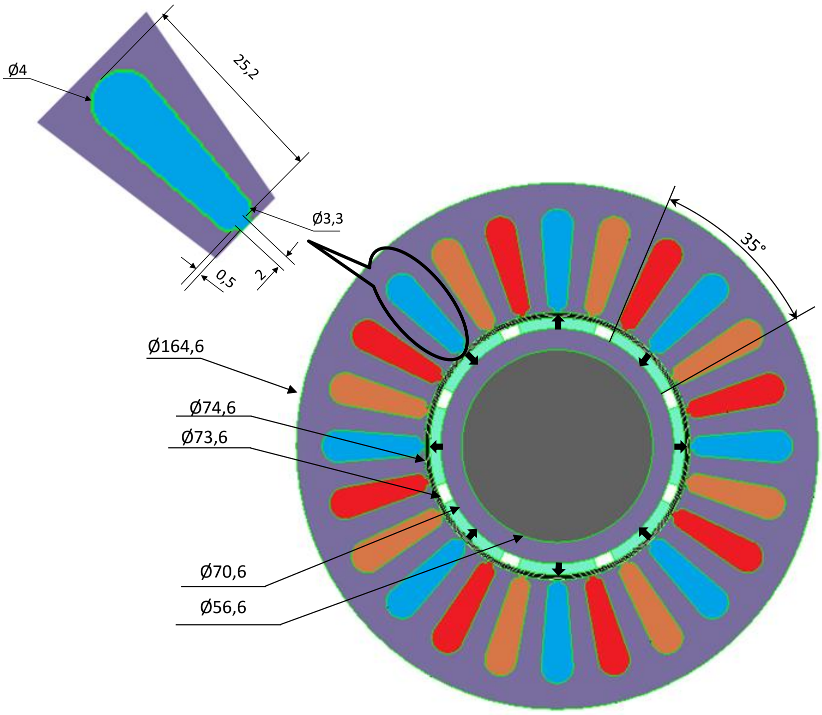

Fig. 2. Cross section view and geometrical parameters of the studied machine

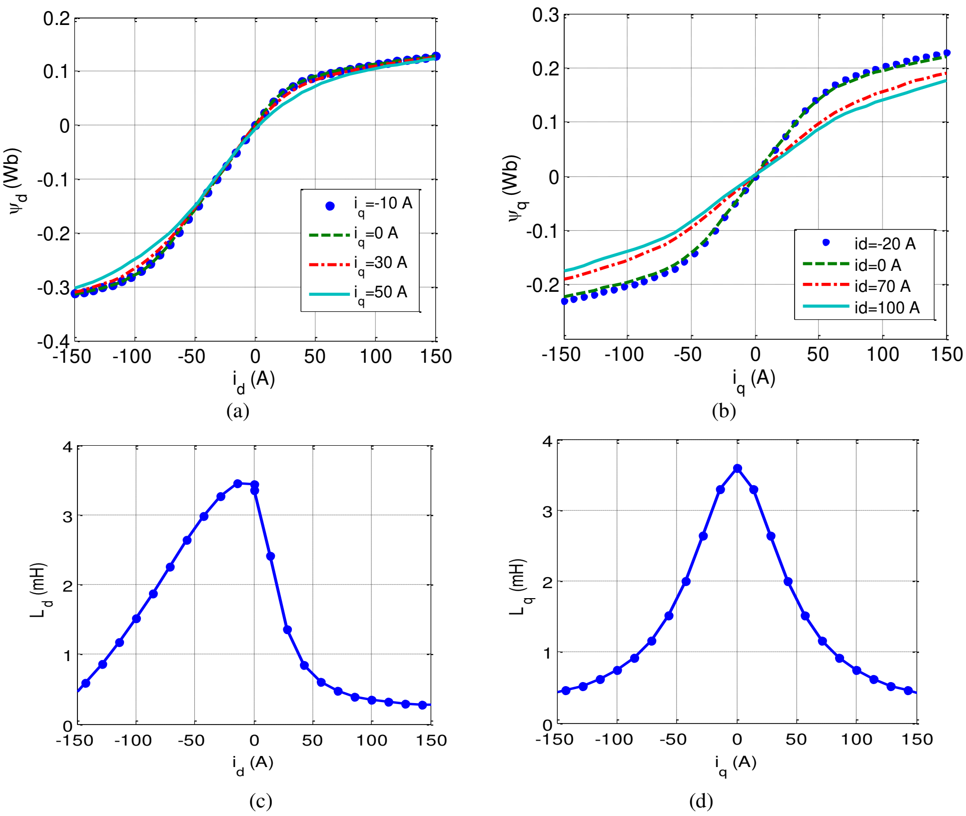

Fig. 3.Flux-current magnetization and dynamic inductances curves of the studied PMSM (a) $\Psi_d(i_d, i_q \text{ constant})$ (b) $\Psi_q(i_q, i_d \text{ constant})$ (c) $L_d(i_d)$ (d) $L_q(i_q)$

Fig. 4 shows the fault current curves computed using the three models, i.e. the classical linear model, the proposed nonlinear model and nonlinear FE. Here, the load torque is set to 20 Nm which leads a high saturation effect. The ratio between the shorted turns and the total turns μ is set to 0.5.

In the simulation results given in Fig. 4.a, the insulation resistance R_f is set to 1 $\mu\Omega$ which leads to a high short-circuit current so to an important saturation level as well. Regarding the results of Fig. 4.a, it can be seen that the proposed model predicts a fault current of about 112 A whereas the nonlinear FE computation gives 139 A (a relative error of about 20%). The linear model underestimates the fault current since it predicts only 81 A (relative error ≈ 40%).

For R_f =0.1 Ω, the results are presented in Fig. 4.b. Again, it can be seen that the proposed model predicts a fault current of 90A and the non-linear FE computation gives a fault current of about 109 A (relative error ≈ 17 %). The linear model underestimates the fault current as it predicts only a value of 69 A (a relative error of about 36 %).

Fig. 4.c presents the fault current obtained for one shorted turn and simulated by the three models. It can be seen here that the proposed model predicts a fault current of about 124 A and the non-linear FE gives a value about 136 A (a relative error of 8%) whereas the linear model underestimates the fault current with a relative error ≈ 12%. In this case, the machine is not saturated so the three models give almost the same results.

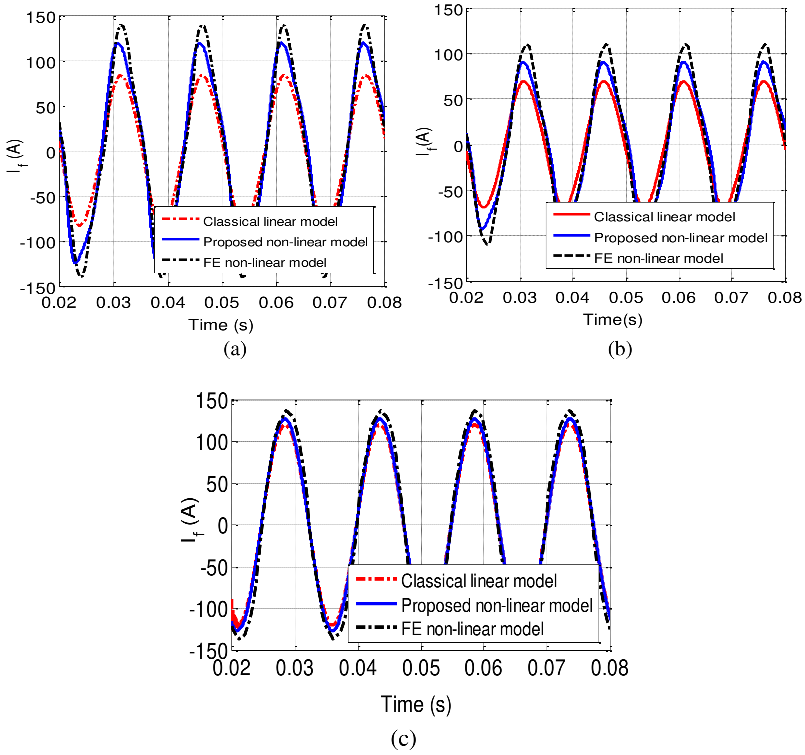

Fig. 4. Fault current with T=20 Nm and for (a) μ=0.5 ,R_f=1 $\mu\Omega$, (b) μ=0.5, R_f=0.1 Ω and (c) 1 shorted turn, R_f=0.1 Ω

In order to study the evolution of the fault severity of the considered machine, the rms value of the fault current is calculated as a function of the insulation resistance R_f . Fig. 5-a shows a comparison between the results obtained by the three different models. Here, the torque and the ratio μ are set to 20 Nm and 0.5 respectively.

It can be seen that the discrepancy between the three models becomes negligible when $R_f > 1\Omega$. Indeed, the fault current in this case is low and the machine is almost under linear operating conditions. For the severe short-circuit case (R_f=0.01) the proposed model predicts an rms fault current value of about 82 A, whereas the nonlinear FE computation gives 87A (a relative error of about 5%). The linear model underestimates the rms value of the fault current since it predicts only 70 A (a relative error of 20 % compared to non-linear FE). The proposed model predicts the fault current with an acceptable accuracy since the relative error compared to the non-linear FE simulations doesn't exceed 5%.

In Fig. 5-b, Fig. 5-c and Fig. 5-d, we have plotted the machine phase currents computed by the three models in the same conditions. As it can be seen, the inter-turn fault results in unbalanced non-sinusoidal phase currents. From the simulation results, the linear model underestimates the phase current i_a (the faulty phase) since it predicts about 85A whereas the non-linear FE model gives about 100 A (relative error of ≈ 15 %). The proposed non-linear model slightly overestimates the magnitude of the phase current i_a with a value of 103 A (relative error of ≈ 5 %).

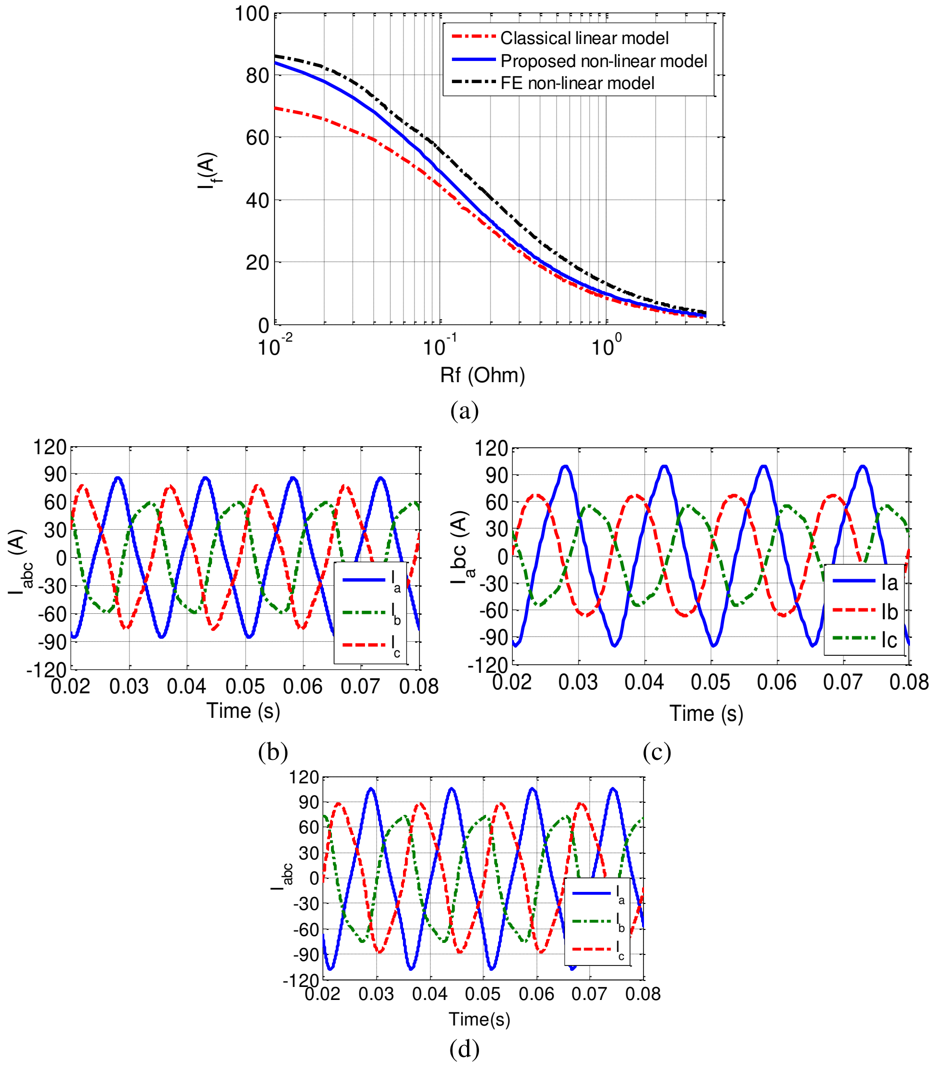

Fig. 5. (a) Short-circuit rms current vs. insulation resistance, R_f (T=22 Nm, μ=0.5)
(b) Classical linear model (c) Non-linear FE model (d) Proposed non-linear model, (R_f =0.1 Ω, T=20 Nm and μ=50%)

B. *Experimental Model Validation (PMSM with concentrated winding)*

The main parameters of this machine in healthy and rated operation are those of Table I. Here, the mutual inductance is neglected (concentrated winding). The parameter k given by (26) is then k=0.

As presented above, we need the non-linear d-q axes fluxes vs. the corresponding d-q currents, Ψ_d(id) and $\Psi_q(i_q)$ to feed into the non-linear model. Here, the geometry of our machine is unknown so we used a simple experimental procedure to obtain these curves as described in [21, 22]. Indeed, it has been shown that a single test allows to obtain the full $\Psi_d(i_d)$ (or $\Psi_q(i_q)$) curves for a constant current i_q (respectively i_d).

To obtain the $\Psi_d(i_d)$ curve for a given i_q current, the experimental procedure (Fig. 6-a) consists of:

- Lock the rotor, so dθ/dt=0,
- Apply an ac step voltage (rectangular wave) while controlling the i_q current to keep it at the desired value,
- Measure and record $u_d(t)$ and $i_d(t)$,

The electrical equation associated to this test procedure is given by (32). The time-dependent flux linkage $\Psi_d(t)$ can be obtained from the recorded voltage $u_d(t)$ and current $i_d(t)$ by integration of (32).

$$u_d(t) = Ri_d(t) + \frac{d\psi_d(t)}{dt} \tag{32}$$

$$\psi_d(t) = \int_0^t \left(u_d(\tau) - Ri_d(\tau)d\tau\right) \tag{33}$$

Fig. 6-b and Fig. 6-c present the applied voltage $u_d(t)$ and the measured current $i_d(t)$ respectively by keeping the current $i_q=0$ for one period. Indeed, the cross saturation effect is neglected.

The flux linkage $\Psi_d(t)$ computed by (36) using the recorded voltage and current given in Fig. 6-b and Fig. 6-c is presented in Fig. 6-d. Hence, at any time t, $\Psi_d(t)$ and $i_d(t)$ are known. Indeed, by eliminating the time form, these two quantities allow the determination of the curve $\Psi_d(i_{d,}\ i_q=0)$ as shown in Fig. 7. It can be seen that the obtained curve is somehow an image of the hysteresis cycle of the ferromagnetic material.

For the obtained complete cycle presented in Fig. 7-a, the average value of current i_d is calculated for each value of the d-axis flux linkage. In this way, the nonlinear characteristic $\Psi_d(i_{d,}\ i_q=0)$ presented in Fig. 7-b is generated. It can be seen that the d-axis magnetizing curve is not symmetrical due to the presence of the PMs flux [23]. A similar procedure can be used to obtain the $\Psi_q(i_q)$ curve for a given i_d current.

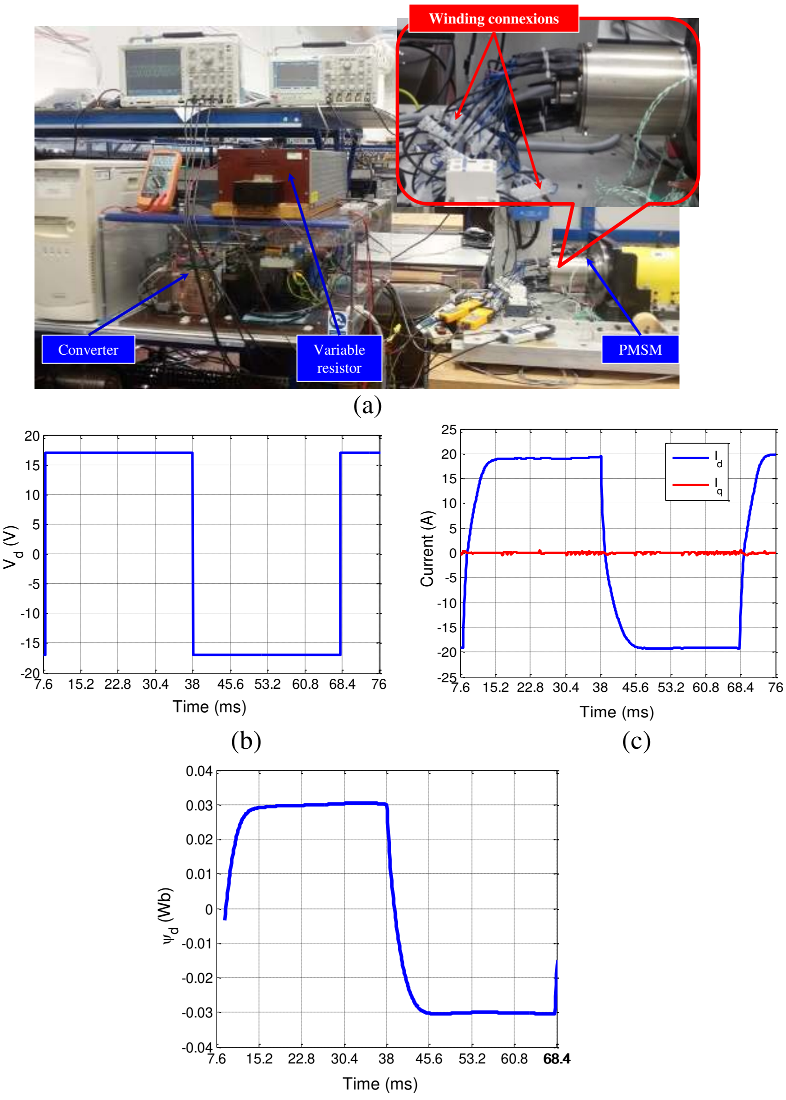

Fig. 6. (a) Photograph of the test bench used for testing the PMSM with concentrated winding (b) The recorded stepwise voltage change V_d, (c) The recorded currents i_d and i_q measured during stepwise voltage and (d) The calculated d- axis flux linkage $\Psi_d(t)$ during the stepwise voltage change V_d for one period.

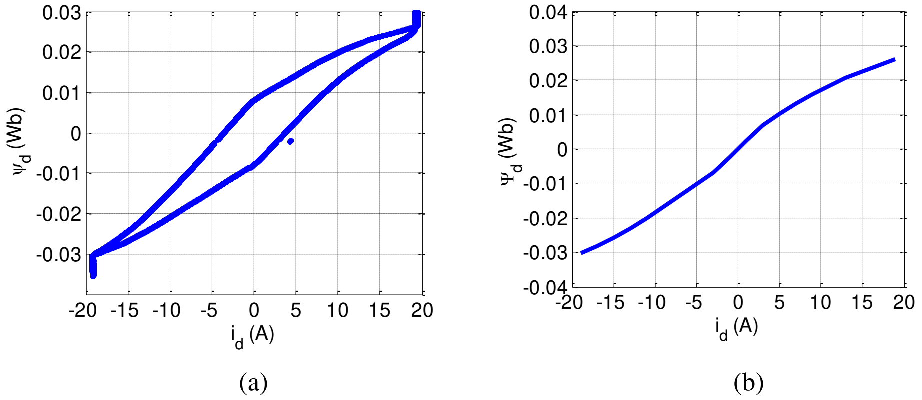

Fig. 7. The non-linear characteristic $\Psi_d(i_d,\ i_q=0)$, (a) one magnetization cycle (b) The characteristic averaged for each Ψ_d.

As shown above, the generated d-axis magnetization curve $\Psi_d(i_d)$ is not symmetrical. The used fitness function is then

$$\Psi_d(i_d)=\begin{cases}5{,}8\ 10^{-3}\arctan(0{,}2329\ i_d)+9{,}97\ .10^{-4}i_d & \text{if } i_d>0\\ 3{,}5\ .10^{-3}\arctan(3{,}42\ .10^{-1}\ i_d)+(1{,}4\ 10^{-3})\ i_d & \text{if } i_d<0\end{cases}\tag{34}$$

In this study, the cross saturation effect is not considered. In fact, the curve $\Psi_d(i_d)$ is measured for $i_q=0$ and the curve $\Psi_q(i_q)$ for $i_d=0$ and approximated by the fitness function (28). As it is shown in Fig. 8-a, the curve $\Psi_q(i_q)$ is symmetrical, so it is approximated by (35). Notice that the $\Psi_q(i_q)$ curve for this surface mounted PM machine under vector control operation the control strategy imposes a null i_d current at base speed.

$$\Psi_q(i_q)=7\ .10^{-4}\arctan(0{,}7669\ i_q)+1{,}9\ 10^{-3}i_q\tag{35}$$

The obtained dynamic d-axis and q-axis current dependent inductances $L_d(i_d)$ and $L_q(i_q)$ are approximated by (36)-(37) and presented in Fig. 8-b and Fig. 8-c. It can be seen that the maximum values of the inductances L_d and L_q are around 2.3 mH and the curve $L_d(i_d)$ is not symmetrical since the d-axis magnetization curve $\Psi_d(i_d)$ is not symmetrical as shown above.

$$\hat{L}_d(i_d)=\begin{cases}\dfrac{1{,}3\ .10^{-3}}{1+0{,}0542\,i_d^{\,2}}+9{,}97\ .10^{-4} & \text{if } i_d>0\\ \dfrac{1{,}2\ .10^{-3}}{1+0{,}117\,i_d^{\,2}}+1\ .10^{-3} & \text{if } i_d<0\end{cases}\tag{36}$$

$$\hat{L}_q(i_q)=\frac{5{,}19\ .10^{-4}}{1+0{,}588\ i_q^{\,2}}+1{,}9\ .10^{-3}\tag{37}$$

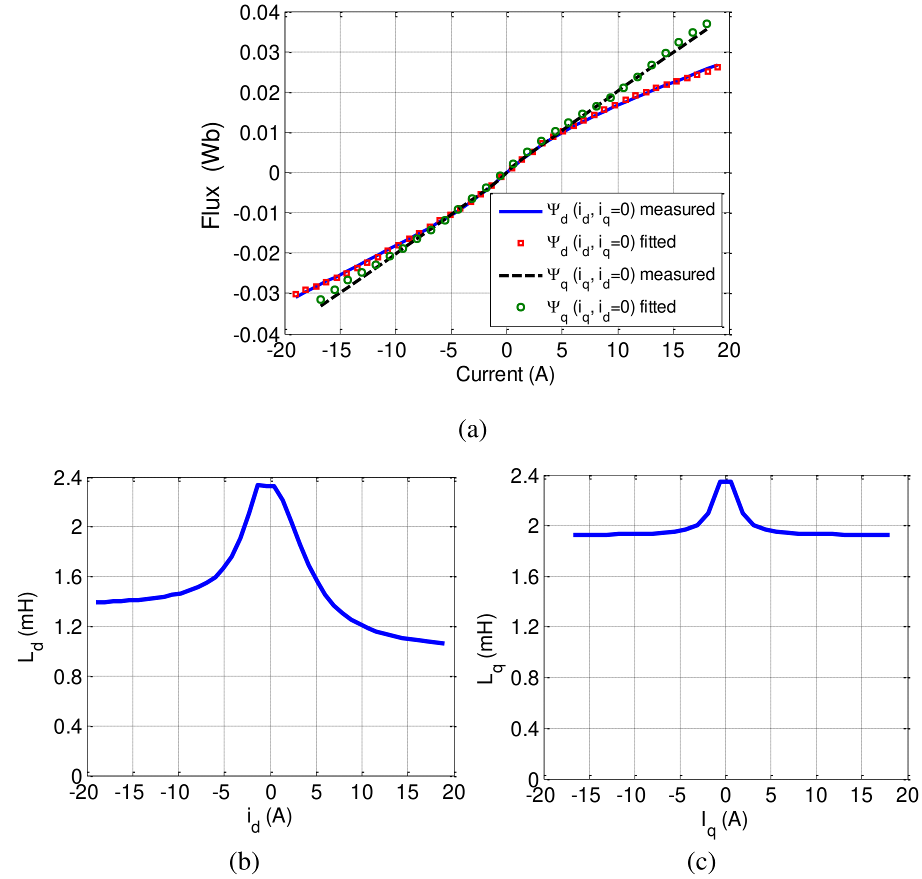

Fig. 8. (a) The generated and approximated non-linear characteristic $\Psi_d(i_d, i_q=0)$ and $\Psi_q(i_q, i_d=0)$, (b) the dynamic d-axis inductance and (c) the dynamic q-axis inductance obtained from fluxes curves approximation

Using the measured and approximated d-axis and q-axis magnetization curves and inductances of the PMSM in healthy case, the faulty machine is simulated in linear and non-linear conditions in MATLAB-SIMULINK environment. The different currents obtained with this simulation are compared with those measured. The fraction of the shorted turns is set to 25%.

This machine is supplied by three phase sinusoidal voltage and operates at 321 rpm. The simulation of the machine in healthy condition can be done by setting a large value of the insulation resistance (1000 Ω). Fig. 9 shows a comparison between the phase currents in healthy case simulated by the proposed non-linear model, those simulated by the linear model and the experimental ones. Here, the developed torque is fixed at 11 Nm. It can be seen that the measurements give a value of 10 A and the proposed model predicts a phase current of 9.6 A (a relative error of 0.3 %). The linear model underestimates the phase currents with a relative error ≈ 4 %. Fig. 10-a shows the fault current curves computed using the proposed non-linear model, the linear model and those measured. Here, the load torque is set to 16 Nm which leads to a higher saturation level than in the previous case; the ratio between the shorted turns and the total turns μ and R_f is set to 0.25. It can be seen that the measured peak fault current and the one computed by the proposed model is about 17 A whereas the one computed by the linear classical model is about 14 A, a relative error of 17%. Fig. 10-b and Fig. 10-c shows the fault current curves computed using the proposed non-linear, the linear models and those measured. Here, the load torque is set to 11 Nm and the ratio between the shorted turns and the total turns μ is set to 0.25.

For the results given in Fig. 10-b, the insulation resistance R_f is set to 1.5 Ω. It can be seen that the proposed model predicts a fault current of about 8 A whereas the measurements give the same value. The linear model underestimates the fault current since it predicts only 6 A.

From the results of Fig. 10-c, the insulation resistance R_f is set to 2.5 Ω. It can be seen here that the proposed model predicts a fault current of about 4.2 A and the measurements give a value of about 4.5 A. The linear model underestimates the fault current as it only gives 4 A.

Notice that a basic vector control is used to control the studied PMSM. In this case, the i_d component of the current is maintained at zero under base speed and the flux linkage Ψ_d doesn't increase with the current i_d. In this case, the results depend on only the load level (the value of the current i_q).

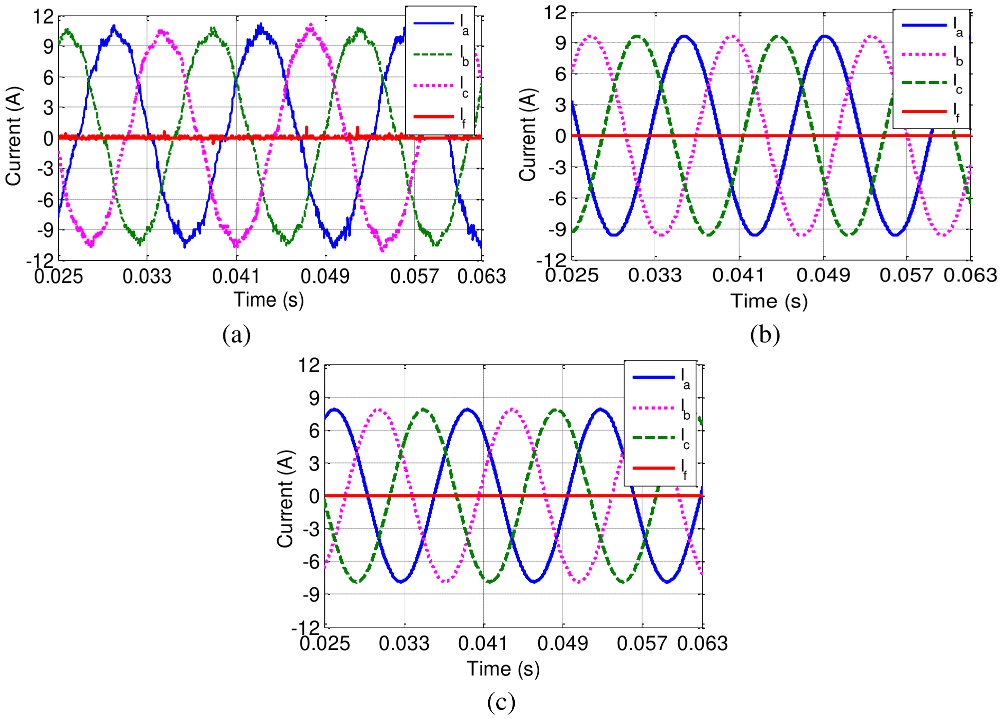

Fig. 9. Phases and fault currents for a healthy machine (a) Measured (b) Proposed non-linear model and (c) Classical linear model

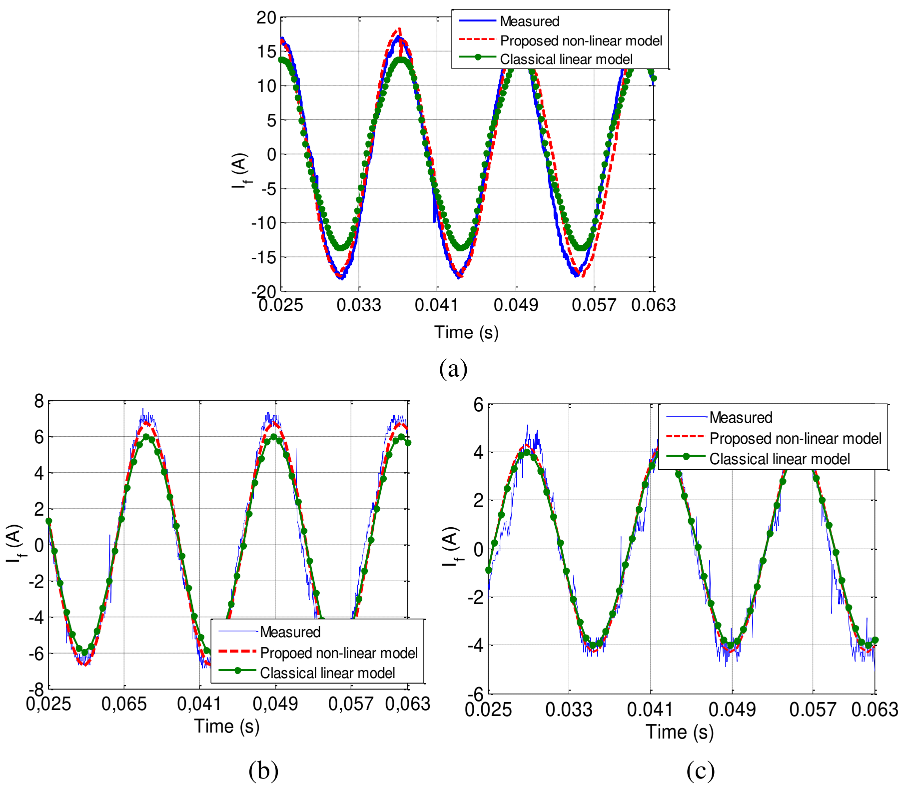

Fig. 10. Fault current comparison:
(a) N=357 rpm, T=16 Nm and for R_f=0.6 Ω, (b) N=321 rpm, T=11 Nm for R_f=1.5 (c) R_f=1.5 Ω (b) N=321 rpm, T=11 Nm for R_f=2.5 Ω

V. Conclusion

A simple dq circuit-based model of PMSM under inter-turn faults which takes into account magnetic saturation has been presented in this paper. The main advantage of this model concerns its easy practical implementation. In fact, all the input parameters of the proposed model are those of the healthy machine data which can be obtained from the machine manufacturer or a simple experimental method. It has been shown that the proposed model predicts the fault current with a reasonable accuracy compared to the FE analyses and to the experimental results. The computation time is very short which makes the model suitable to be incorporated in a global simulation environment of power systems which include electromechanical drives.

REFERENCES

[1] S. B. Lee, R. M. Tallam, and T. G. Habetler, "A robust, on-line turn-fault detection technique for induction machines based on monitoring the sequence component impedance matrix," IEEE Trans. Power Electronics, vol. 18, no. 3, pp. 865-872, May 2003.

[2] D. Diallo, M. E. H. Benbouzid, D. Hamad, and X. Pierre, "Fault Detection and Diagnosis in an Induction Machine Drive: A Pattern Recognition Approach Based on Concordia Stator Mean Current Vector," IEEE Transactions on Energy Conversion, vol. 20, no. 3, pp. 512-519, Sep. 2005.

[3] B. Vaseghi, B. Nahid-Mobarakeh, N. Takorabet, and F. Meibody-Tabar, "Inductance identification and study of PM motor with winding turn short circuit fault," IEEE Trans. Magn., vol. 47, no. 5, pp. 978–981, May. 2011.

[4] N. Leboeuf, T. Boileau, B. Nahid-Mobarakeh, N. Takorabet, F. Meibody-Tabar, and G. CLerc, "Inductance Calculations in PM Motors Under Fault Conditions, " IEEE Trans. Magn, vol. PP, no. 99, p. 1, 2012.

[5] L.Yue, P. Yulong, Y. Yanjun, S. Yanwen, C. Feng, "Increasing the saliency ratio of fractional slot concentrated winding interior permanent magnet synchronous motors," IET Electr. Power Appl., Vol. 9, Iss. 7, pp. 439–448, 2015

[6] O.A. Mohammad, Z. liu, S. Liu, and N. Y. Abed, "Internal Short Circuit Fault Diagnosis for PM Machines Using FE-Based Phase Variable Model and Wavelets Analysis," IEEE Trans. Magn, vol.33, No.4, 2007.

[7] N. Leboeuf, Th. Boileau, B. Nahid-Mobarakeh, N. Takorabet, F. Meibody-Tabar, and G. Clerc, " Estimating Permanent-Magnet Motor Parameters Under Inter-Turn Fault Conditions," IEEE Trans. Magn., vol. 48, no. 2, pp. 963-966, Feb 2012.

[8] A. Mahyob, P. Reghem, G. Barakat, " Permeance Network Modeling of the Stator Winding Faults in Electrical Machines," IEEE Trans. Magn., vol. 45, no. 3, pp. 1820 - 1823, 2009.

[9] B. Sen, J. Wang and P. Lazari, "A Detailed Transient Model of Interior Permanent Magnet Motor Accounting For Saturation under Stator Turn Fault, " IEEE conference on Energy Conversion Congress and Exposition (ECCE), pp. 3548 – 3555, 15-19 Sept 2013.

[10] L. Quéval and H. Ohsaki, "Nonlinear abc-Model for Electrical Machines Using N-D Lookup Table," IEEE Trans. Energy Convers., vol. 99, no. 99, pp. 1–7, 09 Oct 2014.

[11] S. Hemmati, S. S. Kojoori, S. Saied, T. A. Lipo, "Modelling and experimental validation of internal short-circuit fault in salient-pole synchronous machines using numerical gap function including stator and rotor core saturation," IET Electr. Power, Vol. 7, Iss. 5, pp. 391–399, Appl, 2013

[12] P. Ponomarev, I. Petrov, and J. Pyrhönen, "Influence of Travelling Current Linkage Harmonics on Inductance Variation, Torque Ripple and Sensorless Capability of Tooth-Coil Permanent-Magnet Synchronous Machines," IEEE Trans. Magn., vol. 50, no. 1, pp. 8200108, Jan. 2014.

[13] F.P. De Mello, and L.N. Hannett, "Representation of saturation in synchronous machines," IEEE Trans. on Power Systems, Vol. PWRS-1, No. 4, pp. 8-18, Nov. 1986.

[14] N. Bianchi, S. Bolognani, "Magnetic Models of Saturated Interior Permanent Magent Motors based on Finite Element Analysis," 33rd Annual Meeting of the IEEE Industrial Applications Conference, Vol.1., pp.27-34, 12.-15. Oct 1998.

[15] M. Kazerooni, S. Hamidifar, N. C. Kar, "Analytical modelling and parametric sensitivity analysis for the PMSM steady-state performance prediction," IET Electr. Power Appl., Vol. 7, Iss. 7, pp. 586–596, 2013.

[16] IEEE Std 115-1995, Guide: Test Procedures for Synchronous Machines, in IEEE Standards Collection Electric Machinery, Published by IEEE, 1997.

[17] B. Vaseghi, N. Takorabet, and F. Meibody-Tabar, "Fault Analysis and Parameter Identification of Permanent-Magnet Motors by the Finite-Element Method," IEEE Trans. Magn., vol. 45, no. 9, pp. 3290 - 3295, 2009.

[18] S. Williamson and P. Mirzoian, "Analysis of cage induction motcr with stator winding turn faults," IEEE Transactions on Power Apparatus and Systems, vol. 104, no. 7, pp. 1838-1842, 1985.

[19] J. A. Farooq, T. Raminosoa, A. Djerdir, and A. Miraoui, "Modeling and simulation of stator inter-turns faults in permanent magnet synchronous motors," Compel J., vol. 27, no. 4, pp. 887–896, 2008.

[20] R. M. Tallam, T. G. Habetler, and R. G. Harley, "Transient Model for Induction Machines With Stator Winding Turn Faults," IEEE Trans. Ind. Appl, vol. 38, no. 2, pp. 632-637, May 2002.

[21] G. Stumberger, B. Stumberger, D. Dolinar, A. Hamler, M. Trlep, "Evaluation of saturation and cross-magnetization effects in interior permanent magnet synchronous motor," 36th IAS Annual Meeting, IEEE Industry Applications Conference, Vol. 4, pp. 2557 – 2562, 2001.

[22] G. Stumberger, B. Stumberger, D. Dolinarm, "Identification of linear synchronous reluctance motor parameters," IEEE Industry Applications Conference, Vol. 1, pp. 7 – 14, 2000.

[23] W.L.Soong, "Inductactance Measurments for Synchronous Machine, " PEBN#2, May 2008.
Available online http://www.eleceng.adelaide.edu.au/research/power/pebn/